Julian Höcker*, David Kiermasch, Philipp Rieder, Kristofer Tvingstedt, Andreas Baumann and Vladimir Dyakonov

Efficient Solution Processed $CH_3NH_3PbI_3$ Perovskite Solar Cells with PolyTPD Hole Transport Layer

https://doi.org/10.1515/zna-2019-0127
Received April 18, 2019; accepted June 9, 2019; previously published online July 8, 2019

Abstract: The organic and hydrophobic polymer poly[*N*, *N*′-bis(4-butilphenyl)-*N*, *N*′-bis(phenyl)-benzidine] (polyTPD) represents a promising hole transport layer (HTL) for perovskite photovoltaics due to its suitable energy levels, whereby its highest occupied molecular orbital level matches well with the valence band level of methylammonium lead triiodide ($CH_3NH_3PbI_3$, $MAPbI_3$) perovskite. However, processing a perovskite layer from the solution on the surface of this organic material, is found to be difficult due to the surface properties of the latter. In this study, we evaluate efficient p-i-n type $MAPbI_3$ perovskite solar cells employing differently processed polyTPD layers. We found that the surface coverage of the $MAPbI_3$ perovskite layer strongly depends on the preparation method of the underlying polyTPD layer. By varying the solvents for the polyTPD precursor, its concentration, and by applying an optimised two-step perovskite deposition technique we increased both the surface coverage of the perovskite layer as well as the power conversion efficiency (PCE) of the corresponding solar cell devices. Our simple solvent-engineering approach demonstrates that no further interface modifications are needed for a successful preparation of efficient planar photovoltaic devices with PCEs in the range of 15 %–16 %.

Keywords: Hole Transport Materials; Interface Modification; Organolead Triiodide Perovskite Solar Cells; PolyTPD; Solvent Engineering.

***Corresponding author: Julian Höcker,** Experimental Physics VI, Julius Maximilian University of Würzburg, 97074 Würzburg, Germany, E-mail: jhoecker@physik.uni-wuerzburg.de
David Kiermasch, Philipp Rieder and Kristofer Tvingstedt: Experimental Physics VI, Julius Maximilian University of Würzburg, 97074 Würzburg, Germany, E-mail: david.kiermasch@physik.uni-wuerzburg.de (D. Kiermasch); prieder@physik.uni-wuerzburg.de (P. Rieder); ktvingstedt@physik.uni-wuerzburg.de (K. Tvingstedt)
Andreas Baumann: Bavarian Center for Applied Energy Research (ZAE Bayern), 97074 Würzburg, Germany, E-mail: Andreas.Baumann@zae-bayern.de
Vladimir Dyakonov: Experimental Physics VI, Julius Maximilian University of Würzburg, 97074 Würzburg, Germany; and Bavarian Center for Applied Energy Research (ZAE Bayern), 97074 Würzburg, Germany, E-mail: dyakonov@physik.uni-wuerzburg.de. https://orcid.org/0000-0001-8725-9573

1 Introduction

During the last decade perovskite solar cells have attracted a lot of attention and experienced a rapid development in the power conversion efficiency (PCE) from 3.8 % [1] in 2009 to above 23 % [2] in 2019. The remarkable development in this relatively short-time span was enabled by different beneficial material properties such as ambipolar transport with high charge carrier mobilities [3], high absorption coefficients [4] as well as respectable radiative efficiencies [5], which all paved the way to very efficient thin film photovoltaic devices. Recent studies demonstrate that the p-i-n structure is able to compete with the frequently used n-i-p structure in terms of PCE. Different groups already demonstrated that (mesoporous) titanium dioxide, which requires an additional high temperature annealing step during processing, is not necessary to achieve high efficiencies [6–8] due to the introduction of new hole transport layer (HTLs) for p-i-n devices which reduce energy losses at the perovskite/HTL interface and increase the charge collection efficiency of holes. The match between the highest occupied molecular orbital (HOMO) energy level of the HTL and the valence band (VB) of the methylammonium lead triiodide ($MAPbI_3$) perovskite is pivotal in this regard to guarantee an effective HTL to the anode. Furthermore, the HTL should exhibit a high hole conductivity and a high optical transmittance in the photoactive wavelength range of the perovskite absorber material. [9]. So far, poly(3,4-ethylenedioxythiophene) polystyrene sulphonate (PEDOT:PSS) is widely used as HTL for the fabrication of p-i-n perovskite solar cells due to its tunable conductivity, low-temperature solution processability as well as its high optical transmittance

in the visible light wavelength range [10–12]. However, PEDOT:PSS is not an ideal HTL. The semi-metallic nature [13] of the hybrid polymer system leads to an insufficient electron blocking ability, promoting leakage and surface recombination losses at the perovskite/anode interface [14, 15]. In order to minimise these parasitic processes and thus increase the open-circuit voltage (V_{oc}) of the solar cells, different research groups have tried to modify its work function [16] or to use additional electron-blocking interface layers [17]. Conductive polymers such as poly[bis(4-phenyl) (2,4,6-trimethylphenyl) amine] (PTAA) [6, 8, 18] and poly[*N*, *N*′-bis(4-butilphenyl)-*N*, *N*′-bis(phenyl)-benzidine] (polyTPD) [19] are promising alternatives to replace PEDOT:PSS as HTL and are also part of an essential class of amorphous semiconducting polymers. In our work, we focused on the poly(triaryl)amine polyTPD for the fabrication of perovskite solar cells via a solution-processing route. This material embodies a particularly suited HTL due to its beneficial energy levels, whereby its HOMO level of −5.4 eV perfectly matches the VB level of $MAPbI_3$ perovskite with −5.4 eV [19]. This energy level matching therefore provides an essentially ohmichole transport to the indium doped tin oxide (ITO) anode. Moreover, polyTPD acts very well as an electron blocking layer on the basis of its extremely high-lying lowest unoccupied molecular orbital (LUMO) of −2.4 eV. As a consequence, interfacial electron-hole recombination processes are heavily suppressed [15, 20, 21]. Due to these advantages of polyTPD, it was first used as HTL in 2013 with vacuum sublimated $MAPbI_3$ perovskite, demonstrating a V_{oc} of 1.05 V [19]. However, the hydrophobic character of polyTPD has posed a substantial challenge in order to be compatible with a similar solution-processed perovskite solar cell fabrication. The chemical characteristics of the hydrophobic butylene group of polyTPD and the hydrophilic perovskite precursor solution induce a serious dewetting problem during solution processing. To overcome the wettability issue, different groups have tried to improve the surface coverage of the perovskite by using ultraviolet-ozone treatment [22] or poly[(9,9-bis (3-(*N*, *N*-dimethylamino)propyl)-2,7-fluorene)-*alt*-2,7-(9,9-dioctylfluorene)] (PFN) as an amphiphilic interfacial compatibiliser [23]. In the current study, we instead propose a solvent engineering (SE) approach to modify the polyTPD layer in order to achieve the sought-after complete surface coverage of the subsequent perovskite layer without employing additional interfacial layers. Herein, we have applied the two-step thermal annealing-assisted interdiffusion method [24] for producing high-quality $MAPbI_3$ perovskite solar cells.

Our approach thus embodies a simple and low-cost SE-method to modify the polyTPD layer to ensure a complete surface coverage of the subsequent solution-processed $MAPbI_3$ layer. For the SE-method, we used the commercially available and nonpolar solvents 1,2-dichlorobenzene (DCB), chlorobenzene (CB) and toluene (T) to dissolve polyTPD at a temperature of 70 °C. The chemical structures and the physical properties of the used solvents are summarised in the Supplementary Material (Table S1). In addition, we varied the concentration of polyTPD to obtain different thicknesses of the HTL. For pretesting the perovskite wetting properties on the solvent-engineered polyTPD we used a drop of water to mimic the polar solvent *N, N*-dimethylformamide (DMF), which is one of the main solvents for the perovskite precursor. The optical images of water on the solvent-engineered polyTPD in Figure 1a display its hydrophobic surface as compared to the very hydrophilic PEDOT:PSS surface. The overall non-wetting character of water demonstrates that a simple variation of the solvents is in itself not sufficient to prepare uniform $MAPbI_3$ films on the coated polyTPD layer and imposes a challenge in device fabrication. To overcome the wettability issue, we used a 600 mg ml^{-1} lead iodide (PbI_2)/methylammonium iodide (MAI) precursor solution with a molar ratio of 1/0.2, heated to 125 °C to obtain a complete surface coverage (Figure S1) [24]. Figure 1b schematically shows the $MAPbI_3$ film formation on polyTPD. Without any modification, it is not possible to achieve a complete surface coverage of the perovskite layer. By using a SE-method and a modified two-step approach, we were able to fabricate pinhole-free perovskite films on the hydrophobic polyTPD-surface. As a result, perovskite films with areas of 1×1 in.^{2} could be fabricated, when a thin dichlorobenzene-engineered polyTPD layer (see Fig. 1c) is used. Furthermore, the resulting $MAPbI_3$ films exhibited high film quality, as confirmed by scanning electron microscopy (SEM) images. In addition, we obtained high-quality polycrystalline $MAPbI_3$ films on polyTPD layers evident in very sharp peaks at 14.11° and 28.45° shown by the X-ray diffraction spectra (Fig. 1d). This is consistent with the typical tetragonal crystal structure of $MAPbI_3$ in the (110) and (220) planes. Figure 1e shows the absorbance spectrum as well as the steady-state photoluminescence (PL) spectrum of a $MAPbI_3$-film grown on polyTPD. The characteristic of the perovskite structure is given by the sharp absorption edge at around 780 nm which is equivalent to the optical gap of 1.59 eV. PolyTPD itself shows no impact on the absorption behavior of the perovskite due to its transparency and colorlessness. The maximum peak of the PL spectrum was detected at a wavelength of 776 nm and is a further indicator for the

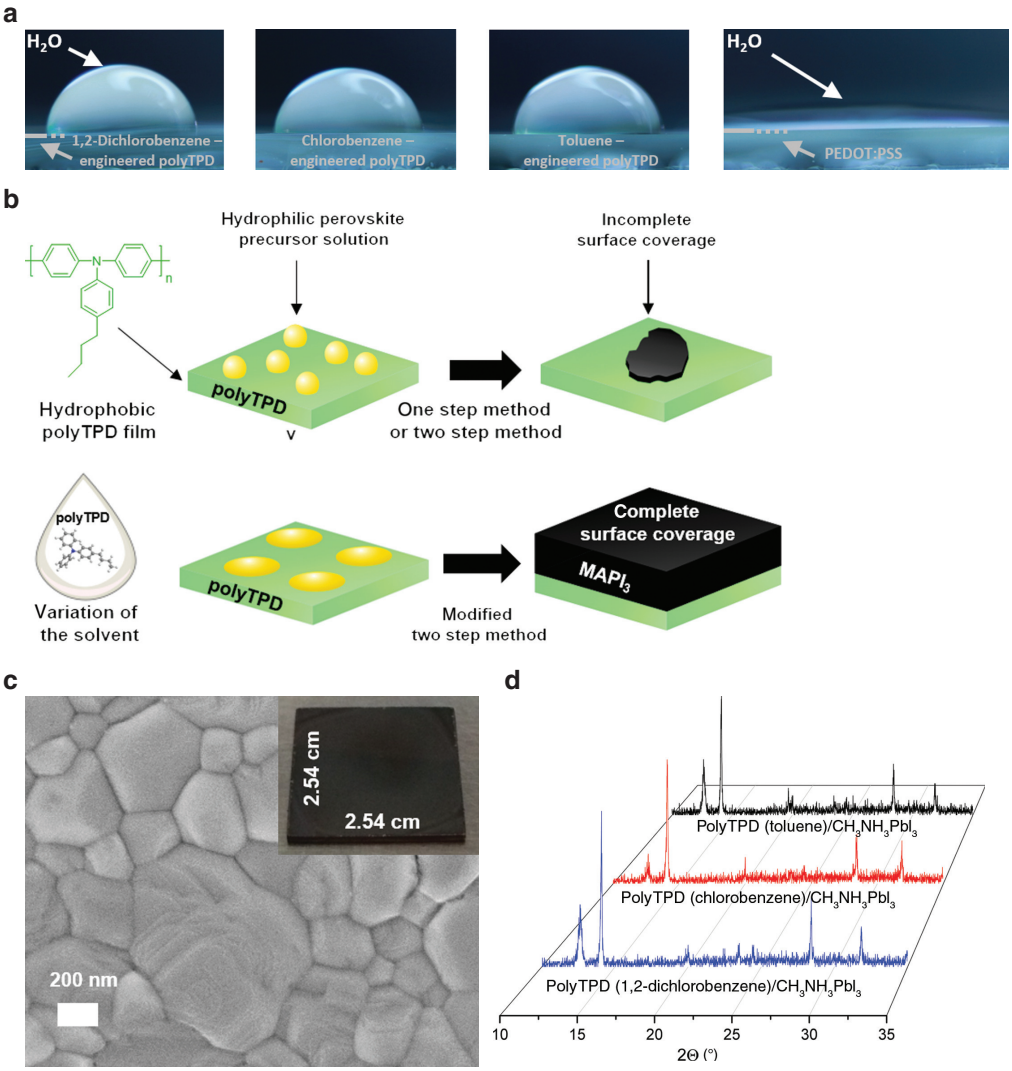

Figure 1: (a) Optical images of water drops on 1,2-dichlorobenzene (DCB), chlorobenzene and dissolved hydrophobic poly[*N*, *N*′-bis(4-butilphenyl)-*N*, *N*′-bis(phenyl)-benzidine] (polyTPD) surface compared to the hydrophilic poly(3,4-ethylenedioxythiophene) polystyrene sulphonate (PEDOT:PSS) surface (polyTPD and PEDOT:PSS surfaces are indicated by dashes). (b) Schematic illustration of the fabrication of pinhole-free methylammonium lead triiodide ($MAPbI_3$) film based on the solvent-engineering approach and the modified two-step thermal annealing-assisted interdiffusion method and (c) the $MAPbI_3$ scanning electron microscopy (SEM) image as well as the corresponding photograph of a fabricated perovskite layer on DCB-engineered polyTPD. (d) X-ray diffraction spectra of $MAPbI_3$ perovskite films grown on solvent-engineered polyTPD. (e) Absorption spectrum and normalised steady-state photoluminescence spectrum of $MAPbI_3$ onto indium doped tin oxide and DCB-engineered polyTPD. (f) Device structure of the $MAPbI_3$ perovskite solar cell using the p-i-n architecture. (g) Cross-section SEM image of the spin-coated layers with [6,6]-phenyl-C61-butyric acid methyl ester ($PC_{61}BM$) on top of the $MAPbI_3$ layer.

successful growth of polycrystalline $MAPbI_3$ thin films on solvent-engineered polyTPD layers. In order to validate our approach, in a next step, we apply the SE technique to solar cells in the p-i-n layout.

Our solar cell configuration is based on the p-i-n device architecture using polyTPD as HTL and $MAPbI_3$ as active layer as shown in Figure 1f. The electron transport layer [6,6]-phenyl-C61-butyric acid methyl ester ($PC_{61}BM$) is deposited from a DCB solution on top of the perovskite followed by vacuum deposited C_{60} layer. Finally, 2,9-dimethyl-4,7-diphenyl-1,10-phenatroline (BCP) is vacuum deposited directly on the C_{60} layer. The metal electrode gold on top of the organic multi-layer system completes the structure of the solar cell device. Figure 1g illustrates the cross-section SEM image of the $MAPbI_3$ perovskite film on the polyTPD substrate with grain sizes up to 350 nm, which is comparable to its film thickness.

We find that not only the SE of the polyTPD precursor, but also an optimisation of its film thickness (via a variation of the concentration from 3, 5, 6, 7, 8 to

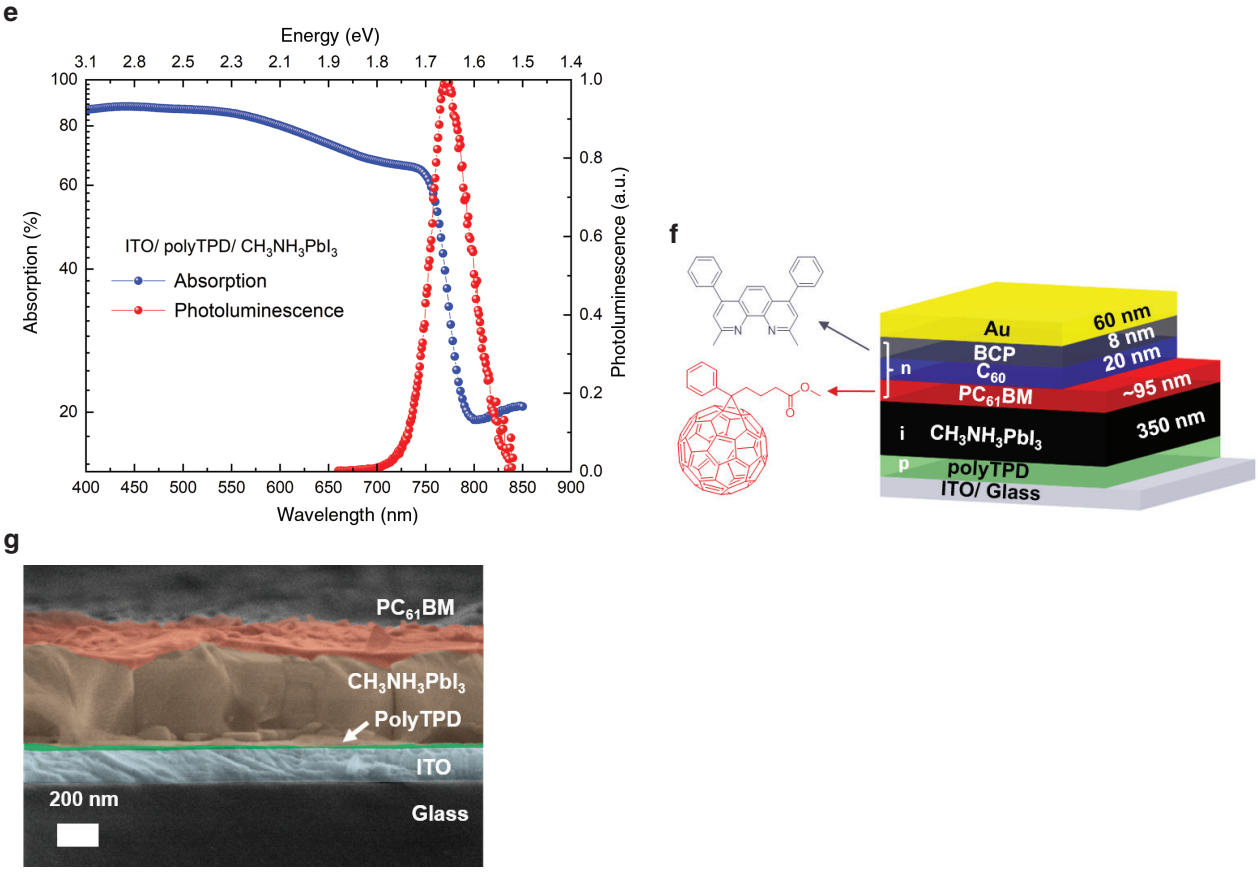

Figure 1: (continued)

10 mg ml^{-1}) is essential to produce pinhole-free $MAPbI_3$ films (see Fig. S2). In fact, we observed differences in the $MAPbI_3$ film formation by using the above-mentioned solvents: the wettability of the perovskite precursor solution on polyTPD dissolved in DCB increases with diminishing concentration, which leads to a complete surface coverage of the $MAPbI_3$ perovskite without the formation of pinholes at low polyTPD-concentrations of 3, 5 and 6 mg ml^{-1}. The $MAPbI_3$ devices with CB-dissolved polyTPD, however, demonstrate an incomplete surface coverage, independent of the polyTPD-concentration. Interestingly, also the $MAPbI_3$ perovskite solar cells based on T-dissolved polyTPD exhibit a continuous pinhole-free perovskite film formation which is comparable to the $MAPbI_3$ devices based on DCB-engineered polyTPD at low concentrations. A possible reason for the wetting/dewetting character of the perovskite film on the different processed polyTPD layers might be the following: polyTPD is solved in three different aromatic hydrocarbons with different boiling points BP (see Supplementary Material Table S1). The solvents are volatile and vaporise completely during the 10-min annealing process, resulting in a dry polyTPD layer. However, the solvents evaporate at different rates while heating the sample up. This might influence the orientation of the polymer chains and the orientation of the hydrophobic butylene group, in detail. The surface morphology of the polyTPD layers is changed by now, and thus leads to a different wetting behaviour of the perovskite film.

Figure 2a–c demonstrates the average of the short-circuit current density J_{SC}, the average of V_{OC} and the average of the fill factor (FF) of the 10 best solar cells as a function of polyTPD concentration and used solvents. In J_{SC} no clear dependence on the choice of solvent can be observed, with the average values ranging from 19.1 to 22.1 mA cm^{-2} and V_{OC} with maximum values ranging from 1.050 to 1.085 V. In stark contrast, the choice of solvent results in significant differences in FF, where devices with DCB-engineered polyTPD show the highest average FF, independent of precursor concentration. At a low polyTPD concentration, the DCB-based devices reach an average FF of 68 % as compared to the CB- and T-engineered polyTPD based devices with the highest average FF values of 62 % and 58 %, respectively. In fact, this variation in FF

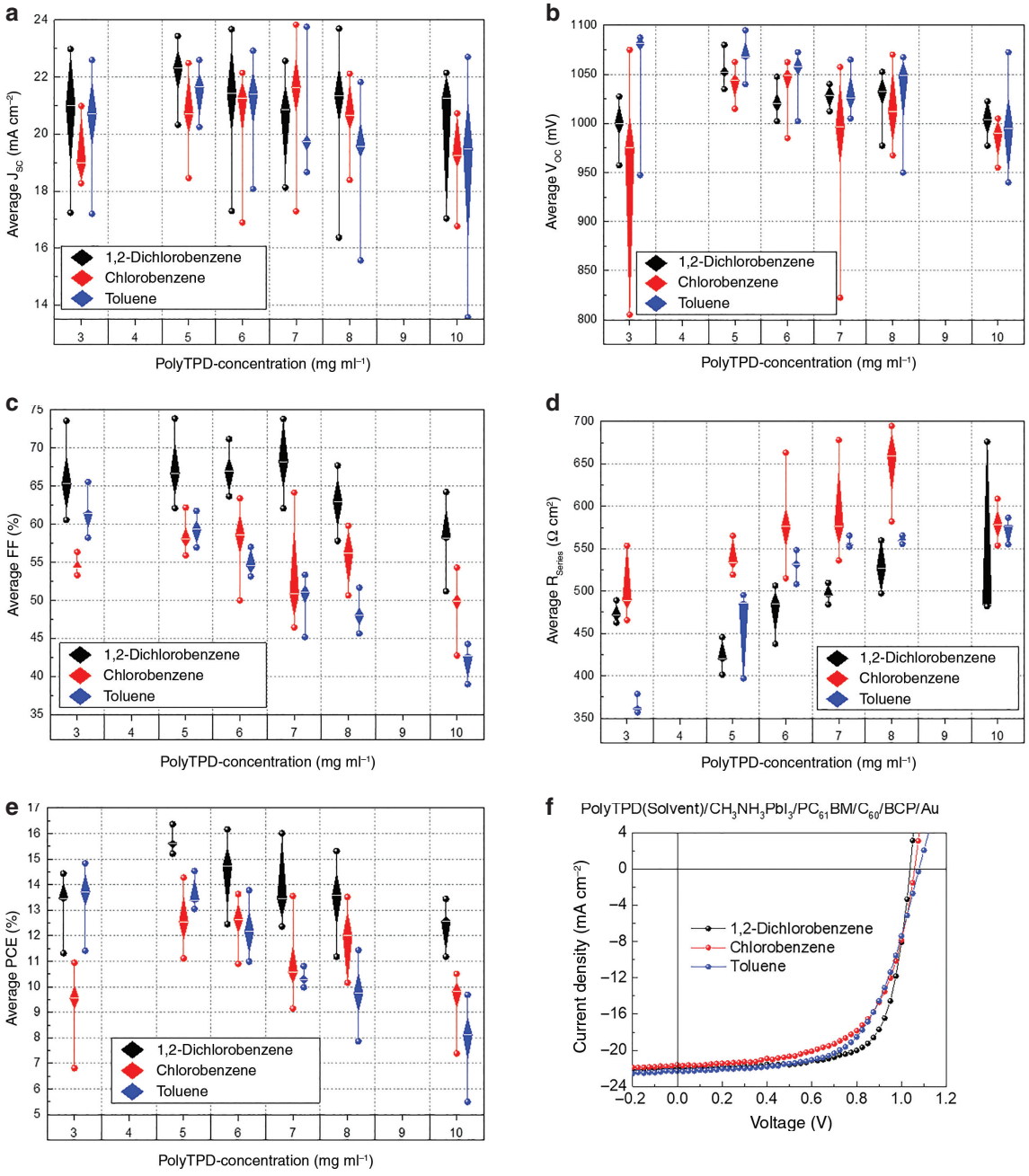

Figure 2: (a) Average of J_{SC}, (b) of V_{OC}, and (c) of fill factor (FF) of the 10 best solar cells as function of the polyTPD concentration. (d) Average R_{Series} of 5 polyTPD based solar cell devices. (e) Average of power conversion efficiency of the 10 best solar cells for each polyTPD concentration. (f) J–V characteristics of the best solvent-engineered solar cells.

directly translates to the superior device performance of DCB-engineered devices, with PCEs of above 16 % for an optimized thickness, as can be seen in Figure 2e.

Moreover, the increase in polyTPD precursor concentration and, therefore, the increase in polyTPD layer thickness leads to an increase in series resistance R_{Series} of all devices, from a minimum value of 363 Ω cm^2 up to a maximum value of 651 Ω cm^2, as summarised in Figure 2d. This, in turn, causes a substantial drop in FF in all presented solar cells for concentrations exceeding 5 mg ml^{-1}, as visible in Figure 2c. The J–V curves of all perovskite solar cells under illumination with varying polyTPD concentration are shown in Figure S3. In summary, the devices with DCB-engineered polyTPD using a concentration of 5 mg ml^{-1} show the highest average PCE with reproducible values in the range of 15.6 %–16.4 %. For a better comparison, the J–V characteristics of the best respective solvent-engineered solar cells under

illumination are demonstrated in Figure 2f. In particular, the solar cell containing DCB-engineered polyTPD exhibited the highest PCE of 16.4 % with V_{OC} of 1.04 V, J_{SC} of 21.8 mA cm^{-2}, and a high FF of 72.3 %. This is obtained for a low polyTPD-concentration of 5 mg ml^{-1}, which leads to a perfect and complete surface coverage of the subsequently deposited $MAPbI_3$ perovskite film.

To verify the applicability of our SE approach to upscaling, we have manufactured solar cells on 1-inch substrates. Figure 3a shows the photograph of an 1 × 1 in.^{2} substrate containing four perovskite solar cells based on DCB-engineered polyTPD. Each of the solar cells has a total active area of 0.54 cm^2. All devices exhibit high PCE values with only small deviations, with the best performing solar cell displaying a PCE of 15.15 % with a V_{OC} as high as 1.085 V (Fig 3b), only slightly lower than for small-area devices with active areas of below 0.09 cm^2. The possibility to fabricate solution-processed perovskite solar cells with untreated polyTPD as HTL allows for a direct comparison to otherwise identical solar cells based on the commonly used HTL PEDOT:PSS, as well as a bilayer stack of both HTLs, with regard to their photovoltaic performance: the *J*–*V* characteristics of the devices are shown in Figure 3c. Compared to the previously discussed polyTPD-only record device (based on DCB as a solvent), the PEDOT:PSS solar cell demonstrates a higher FF of 80.3 %, but a substantially lower V_{OC} of only 0.903 V, resulting in a PCE of 15.51 %. In order to compare solar cells with polyTPD (DCB) and PEDOT:PSS as HTL in terms of stability, we measured *J*–*V* curves over 40 days. The normalised J_{SC}, V_{OC}, *FF* and PCE over time can be found in the Supplementary Material in Figure S4a–d. As can clearly be seen, the PCE of the solar cell with polyTPD is stable over time whereas the PCE of the PEDOT:PSS solar cell drops due to the decrease of *FF*.

If both HTLs are combined in a bilayer device, where polyTPD is processed on PEDOT:PSS, a high V_{OC} of 1.07 V will be achieved. Nonetheless, the poor FF of 63.6 % limits the device performance to only 15.5 %. This 130–160 mV increase in V_{OC} can be explained by the superior ability of polyTPD to block electrons compared to PEDOT:PSS, underlining its great potential for further use in solution processed perovskite solar cells. This property results in another advantage of polyTPD as HTL, as can be seen in the comparison of the respective dark *J*–*V* curves in Figure 3d: PEDOT:PSS as HTL displays the lowest parallel

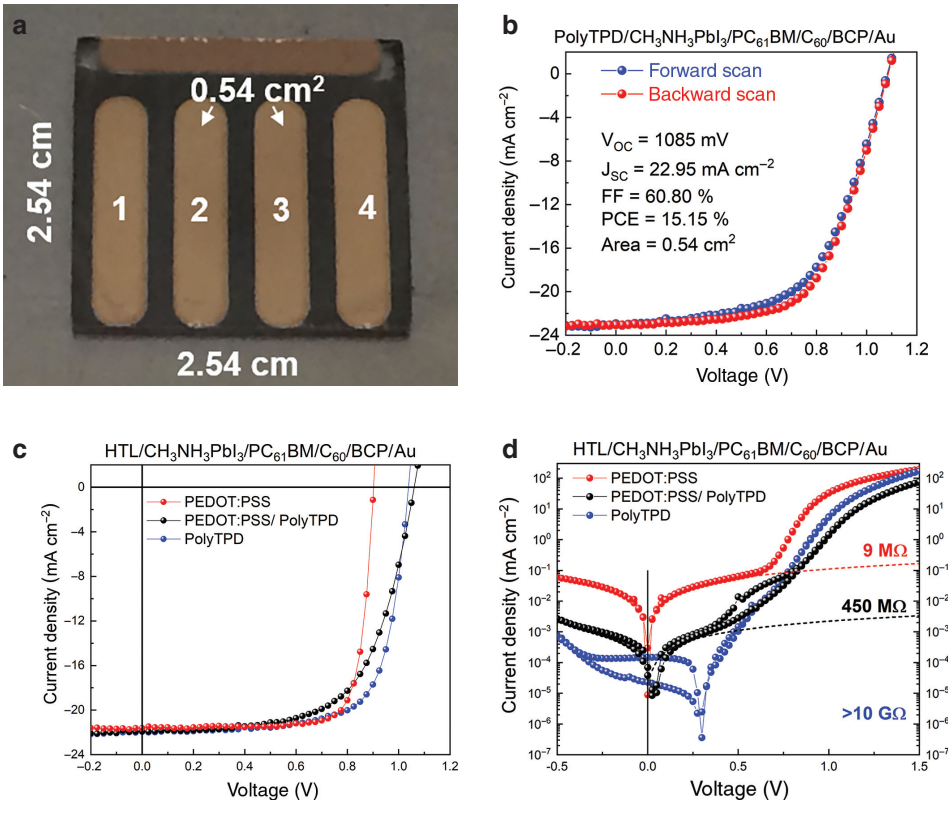

Figure 3: (a) Photograph of an $MAPbI_3$ perovskite solar cell fabricated on a large substrate (1 × 1 in.^{2}). (b) *J*–*V* curve of the best $MAPI_3$ perovskite solar cell. Comparison of *J*–*V* curves of the best (c) illuminated and (d) dark $MAPbI_3$ solar cells with different hole transport layer. (d) The extracted values of R_{Shunt}.

resistance R_{Shunt} of 9 MΩ of the three devices, compared to the $MAPbI_3$ solar cell based on PEDOT:PSS/polyTPD with R_{Shunt} of 450 MΩ and the neat polyTPD device with a remarkably high R_{Shunt} of above 10 GΩ. As a consequence, leakage currents are significantly suppressed, which enables the solar cell to operate under low light conditions as well, as we have previously shown for fully evaporated perovskite solar cells [15]. We note that the retaining V_{OC} visible for the polyTPD-only device is caused by very weak stray light, which was present during all dark J–V measurements. Nonetheless, it can only be seen in the polyTPD device for the reasons discussed above.

In conclusion, we have presented a route to process planar p-i-n $MAPbI_3$ perovskite devices with polyTPD as HTL. Without the use of an interfacial layer such as PFN, we were able to process efficient perovskite devices by varying the solvent, the polyTPD concentration, and by applying a modified two-step-technique. First, we optimised the wettability of the perovskite precursor on the polyTPD layer, which was prepared by varying solvents and concentrations to achieve full surface coverage on the substrate. The best performing $MAPbI_3$ perovskite device with a high FF of 74 % was realised using a DCB-engineered polyTPD layer with a concentration of 5 mg ml^{-1}. Moreover, this SE approach allowed to prepare pinhole free $MAPbI_3$ perovskite devices on 1 × 1 $in.^2$ substrates with PCE values above 15 %. We also demonstrate that polyTPD HTL prepared in this way has exceptional hole-selective properties under low-light conditions due to high R_{Shunt}. Our work offers an alternative approach to the processing planar p-i-n $MAPbI_3$ solar cells from the solution without the need of vacuum depositing $MAPbI_3$ or the use of additional interface layers to prevent layer dewetting.

2 Experimental Section

2.1 Device Fabrication

The spin-coating process was implemented in a nitrogen-filled glovebox with oxygen and water levels below 1 ppm. Pre-patterned ITO (Visiontek Systems Ltd., Upton Chester, Cheshire, UK) was cleaned in detergent and subsequently sonicated in deionized water, acetone and isopropanol for 10 min each. After this, the substrates were exposed to an O_2-plasma for 30 s. PolyTPD (1-Material, Dorval, Quebec, Canada, M_W = 45,800, M_n = 18,320, PDI = 2.5) was dissolved in the solvents DCB, CB and T (Merck KGaA/Sigma Aldrich, Darmstadt, Germany; anhydrous), overnight at 70 °C under constant stirring. The polyTPD-precursor was spin-coated onto the cleaned substrates at 5000 rpm for 30 s. The samples were annealed at 110 °C for 10 min. The $MAPbI_3$ films were fabricated based on the interdiffusion method. Thereby, PbI_2 (TCI Deutschland GmbH, Mergenthalerallee, Eschborn, Germany; 99.999 %, trace metal basis) and MAI (Luminescence Technology Corp., Xizhi, New Taipei City, Taiwan; 99 %) were spun onto the substrate consecutively, followed by a solvent annealing process to recrystallise the small-size crystals into large perovskite grains with reduced pinhole formation [25]. The concentration of PbI_2 was fixed at 600 mg ml^{-1} with a molar fraction of 0.2 mol MAI. The precursor layers were spin coated with 125 °C preheated PbI_2/MAI solution in DMF (Merck KGaA/Sigma Aldrich, Darmstadt, Germany; anhydrous) at a spin speed of 5000 rpm to obtain a better wettability [24]. Thereafter, the PbI_2/MAI films were thermally annealed at 70 °C for 10 min. The concentration of MAI was fixed at 40 mg ml^{-1}, dissolved in isopropanol (Merck KGaA/Sigma Aldrich, Darmstadt, Germany; anhydrous). The deposition of MAI film was taken at 3400 rpm. To ensure a controlled crystallisation, the stacked perovskite films were annealed at 100 °C for 60 min in boxes in a solvent atmosphere of dimethyl sulfoxide (Merck KGaA/Sigma Aldrich, Darmstadt, Germany; anhydrous). Next, $PC_{61}BM$ (Solenne BV, Zernikepark, Groningen, The Netherlands; 99 %) was dissolved in DCB with a concentration of 20 mg ml^{-1} and spin-coated on top of the $MAPbI_3$ layer with a spin speed of 6000 rpm. The films were annealed at 100 °C for 60 min. After this, C_{60} (Solenne BV, Zernikepark, Groningen, The Netherlands; 99.5 %) was thermally evaporated onto the substrate with a final thickness of 20 nm. The solar cell devices were completed by the evaporation of 8 nm BCP (Merck KGaA/Sigma Aldrich, Darmstadt, Germany; 99.5 %) and a 60 nm thick gold electrode. The thermal evaporation process was realised under high vacuum with a pressure of 10^{-7} mbar.

2.2 Characterisation

HTL/$MAPbI_3$ films were imaged with a SEM Ultra plus by Carl Zeiss Microscopy GmbH (Heidelberg, Germany) using a secondary electron detector. The measurements were performed in high vacuum. The J–V characteristics of the devices were measured in a nitrogen-filled glovebox under conditions of AM 1.5 G global spectral irradiance of 100 mW cm^{-2} with a Xenon-lamp-based solar simulator (ORIEL 68811, Newport Corporation, Oriel Instruments, CA, USA). Keithley MODEL 2612 B (Tektronix GmbH Keithley Instruments, Germering, Germany) was applied for recording the J–V measurements. The exact illumination intensity was calibrated with a reference silicon solar cell (VLSI Standards, Inc., Five Technology Drive, Milpitas, CA, USA). The solar cells were directly measured (forward and backward scan) without any pretreatments after the evaporation process. The devices were stored in sample boxes in a nitrogen-filled glovebox to study the stability. The values of V_{OC}, J_{SC} and FF were obtained by the backward-scan of the J–V measurements.

Acknowledgements: We would like to thank Stephan Braxmeier from the Bavarian Center for Applied Energy Research (ZAE Bayern) for taking the SEM images. Authors acknowledge the Federal Ministry of Research and Education (BMBF) for funding through the grant HYPER with Grant Agreement 03SF0514. V.D. acknowledges funding from the Bavarian Collaborative Research Program "Solar Technologies Go Hybrid" (SolTech). K.T. acknowledges the DFG funding under 382633022. A. B. works at the ZAE

Bayern, financed by the Bavarian Ministry of Economic Affairs, Regional Development and Energy.

References

[1] A. Kojima, K. Teshima, Y. Shirai, and T. Miyasaka, J. Am. Chem. Soc. **131**, 6050 (2009).
[2] R. H. Friend, F. Deschler, L. M. Pazos-Outón, M. Abdi-Jalebi, and M. Alsari, Sci.Video Protocols **1**, 1 (2019).
[3] L. M. Herz, ACS Energy Lett. **2**, 1539 (2017).
[4] P. Löper, M. Stuckelberger, B. Niesen, J. Werner, M. Filipič, et al., J. Phys. Chem. Lett. **6**, 66 (2015).
[5] K. Tvingstedt, O. Malinkiewicz, A. Baumann, C. Deibel, H. J. Snaith, et al., Sci. Rep. **4**, 6014 (2014).
[6] Q. Wang, Q. Dong, T. Li, A. Gruverman, and J. Huang, Adv. Mater. **28**, 6734 (2016).
[7] C. Momblona, L. Gil-Escrig, E. Bandiello, E. M. Hutter, M. Sessolo, et al., Energy Environ. Sci. **9**, 3456 (2016).
[8] M. Stolterfoht, C. M. Wolff, Y. Amir, A. Paulke, L. Perdigon-Toro, et al., Energy Environ. Sci. **10**, 1530 (2017).
[9] T. Liu, K. Chen, Q. Hu, R. Zhu, and Q. Gong, Adv. Energy Mater. **6**, 4173 (2016).
[10] W. Zhang, B. Zhao, Z. He, X. Zhao, H. Wang, et al., Energy Environ. Sci. **6**, 1956 (2013).
[11] D. H. Sin, H. Ko, S. B. Jo, M. Kim, G. Y. Bae, et al., ACS Appl. Mater. Interfaces **8**, 6546 (2016).
[12] Z. Yu, Y. Xia, D. Du, and J. Ouyang, ACS Appl. Mater. Interfaces **8**, 11629 (2016).
[13] O. Bubnova, Z. U. Khan, H. Wang, S. Braun, D. R. Evans, et al., Nat. Mater. **13**, 190 (2014).
[14] Y. Hou, W. Chen, D. Baran, T. Stubhan, N. A. Luechinger, B. Hartmeier, et al., Adv. Mater. **28**, 5112 (2016).
[15] K. Tvingstedt, L. Gil-Escrig, C. Momblona, P. Rieder, D. Kiermasch, et al., ACS Energy Lett. **2**, 424 (2017).
[16] K.-G. Lim, H.-B. Kim, J. Jeong, H. Kim, J. Y. Kim, et al., Adv. Mater. **26**, 6461 (2014).
[17] Q. Xue, G. Chen, M. Liu, J. Xiao, Z. Chen, et al., Adv. Energy Mater. **6**, 1502021 (2016).
[18] Q. Wang, C. Bi, and J. Huang, Nano Energy **15**, 275 (2015).
[19] O. Malinkiewicz, A. Yella, Y. H. Lee, G. M. Espallargas, M. Graetzel, et al., Nat. Photon **8**, 128 (2014).
[20] R. S. Sprick, M. Hoyos, M. S. Wrackmeyer, A. V. Sheridan Parry, I. M. Grace, et al., J. Mater. Chem. C **2**, 6520 (2014).
[21] O. Malinkiewicz, C. Roldán-Carmona, A. Soriano, E. Bandiello, L. Camacho, et al., Adv. Energy Mater. **4**, 1400345 (2014).
[22] X. Xu, C. Ma, Y. Cheng, Y.-M. Xie, X. Yi, et al., J. Power Sources **360**, 157 (2017).
[23] J. Lee, H. Kang, G. Kim, H. Back, J. Kim, et al., Adv. Mater. **29**, 1606363 (2017).
[24] C. Bi, Q. Wang, Y. Shao, Y. Yuan, Z. Xiao, et al., Nat. Commun. **6**, 7747 (2015).
[25] Z. Xiao, Q. Dong, C. Bi, Y. Shao, Y. Yuan, et al., Adv. Mater. **26**, 6503 (2014).

Supplementary Material: The online version of this article offers supplementary material (https://doi.org/10.1515/zna-2019-0127).